

## Arc-heater as an Atomic Oxygen Generator

Makoto MATSUI<sup>1</sup>, Satoshi OGAWA<sup>2</sup>, Yasuhisa ODA<sup>1</sup>, Ittoku YAMAJI<sup>2</sup>, Kimiya KOMURASAKI<sup>3</sup>,  
 and Yoshihiro ARAKAWA<sup>4</sup>

<sup>1,3</sup>Department of Advanced Energy, The University of Tokyo

<sup>2,4</sup>Department of Aeronautics and Astronautics, The University of Tokyo  
 Hongo 7-3-1, Bunkyo, Tokyo 113-0033, Japan

### Abstract

Number density distributions of metastable atomic oxygen in arcjet-type arc-heater plumes were obtained by laser absorption spectroscopy. The oxygen was found to be located off axis at the nozzle exit, and diffuses from outside toward centerline in the plume, resulting in the low number density. Numerical simulation calculated for the arc-heater plume also indicates the same diffusion process of the oxygen as the experimental one. Therefore, for the enhancement of the oxygen dissociation, the oxygen injection-port was improved so as that oxygen passes through a high temperature cathode-jet region.

### 1. Introduction

In developing Thermal Protection Systems for reentry vehicles, arc-heaters are often used to simulate reentry conditions. Arcjet type arc-heaters<sup>1-3)</sup> and segmented cathode type arc-heaters<sup>4,5)</sup> are widely used. The segmented cathode type has an advantage of high input power because it can sustain long arc discharge. However, it takes several hours for maintenance after a few minutes operation. On the other hand, the arcjet type requires almost no maintenance after several-hour operation. Therefore, arcjet type arc-heaters are convenient for basic TPS studies.

However, their exact plume conditions are mostly unknown because they are usually in strong thermo-chemical nonequilibrium. Although non-intrusive spectroscopic methods such as emission spectroscopy and Laser Induced Florescence have been actively applied to the characterization of such high enthalpy plumes, and the excitation, vibration, and rotational temperatures of atoms and molecules in the plumes are gradually clarified,<sup>6-9)</sup> it is still difficult to measure the chemical compositions by these spectroscopic methods.

Recently, atomic oxygen in a high enthalpy flow is found to play important roles in TPS tests through the heat-flux enhancement by recombination reactions and the active-passive oxidation.<sup>10)</sup>

In this study, number density distributions of meta-stable atomic oxygen in the conventional arcjet type arc-heater plumes were measured along with CFD analysis. Next, for the enhancement of oxygen

dissociation, a new arcjet type arc-heater has been developed and its plume properties were tested.

### 2. Conventional Arcjet type Arc-heater

#### 2.1 Measurement Method

##### 2.1.1 Arc-heaters

The schematics of arcjet type arc-heaters developed at the Japan Ultra-high Temperature Materials research center (JUTEM) and at the University of Tokyo are shown in Figs. 1 and 2, respectively. In both of the arc-heaters, inert gas such as argon or nitrogen is supplied from the base of cathode rod. Oxygen is added at the constrictor part to prevent the cathode from oxidization.

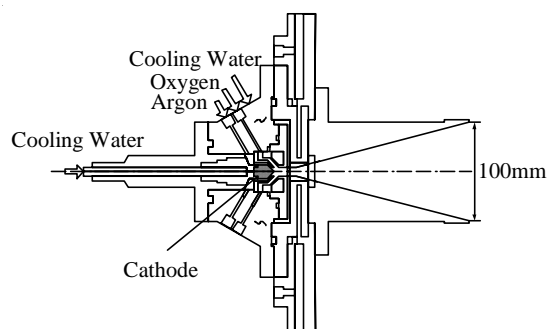


Fig. 1 JUTEM arc-heater

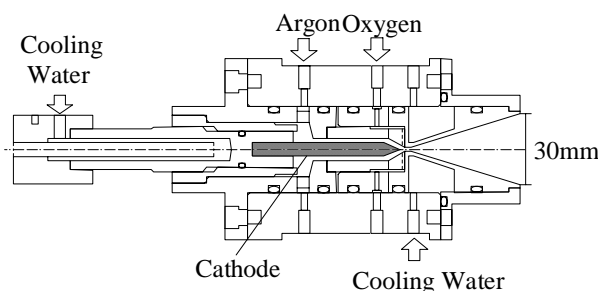


Fig. 2 The University of Tokyo arc-heater

<sup>1,2</sup>Graduate student

<sup>3</sup>Associate Professor, Senior Member AIAA

<sup>4</sup>Professor, Senior Member AIAA

### 2.1.2 Principle of Laser absorption spectroscopy

In this study, the number density of atomic oxygen is measured using the absorption profile of the OI transition from  $3s^5S$  to  $3p^5P$  at the wavelength of 777.19nm. Here, a brief description of the theory of laser absorption spectroscopy is summarized. More details are shown in reference [11,12].

#### Number density

Number density of an absorption state  $n_1$  is related to integrated absorption coefficient  $K$ , as

$$K = \int_{-\infty}^{\infty} k_{\nu} d\nu = \frac{\lambda^2}{8\pi} \frac{g_2}{g_1} A_{21} n_1. \quad (1)$$

Here,  $k_{\nu}$  is absorption coefficient at the frequency of  $\nu$ ,  $\lambda$  is absorption wavelength,  $g$  is statistical weight, 1 and 2 denotes the lower and upper states and  $A$  is Einstein coefficient. At 777.19nm,  $g_1=5$ ,  $g_2=7$  and  $A_{21}=3.69 \times 10^7 s^{-1}$ .

#### Translational temperature

In low-pressure plasma, Doppler broadening is generally dominant and translational temperature  $T$  is related to a full width at the half maximum  $\Delta\nu_D$  of an absorption profile, expressed as,

$$\Delta\nu_D = \frac{\sqrt{8R \ln 2}}{\lambda_0} \sqrt{\frac{T}{M}} \quad (2)$$

Here,  $c$  is the velocity of light,  $R$  is gas constant,  $\lambda_0$  is the center frequency of the absorption and  $M$  is the atomic weight of the absorbing atom.

### 2.1.2 Experimental apparatus and conditions

The schematic of measurement system is shown in Fig. 3. A tunable diode-laser with an external cavity was used as a laser oscillator. The laser beam is divided into three beams by beam splitters. The first beam is directly detected by a photo-detector as a reference signal. The second is detected through an etalon, whose free spectral range is 1 GHz. The third is lead to a window of vacuum chamber through a multimode optical fiber. The fiber output is mounted on a one-dimensional traverse stage to scan the plume in the radial direction of the plume. At the other side of the chamber, the laser beam is focused on a detector using a parabola mirror. This makes it possible to detect the probe laser without synchronizing the detector position with the laser scanning. The test conditions are listed in Table 1.

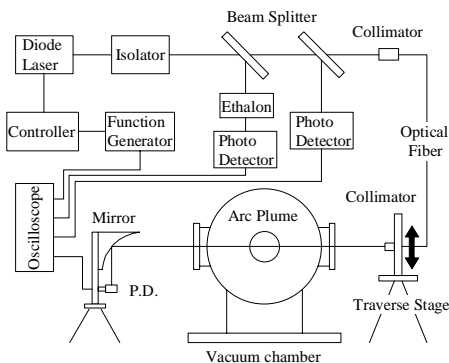


Fig. 3 Schematic of measurement system

Table 1 Test conditions.

	Institute	Gas flow	Specific enthalpy	Back pressure
Case1	JUTEM	Ar: 20[slm] O <sub>2</sub> : 5[slm]	6.1 [MJ/kg]	38 [Pa]
Case2	The Univ. of Tokyo	Ar: 6[slm] O <sub>2</sub> : 1[slm]	3.3 [MJ/kg]	26 [Pa]

## 2.2 Experimental Results

The number density distribution of metastable atomic oxygen in the JUTEM arc-heater plume is shown in Fig. 4. Here,  $z$  and  $r$  are defined by the cylindrical coordinate and origin is taken at the center of nozzle exit.

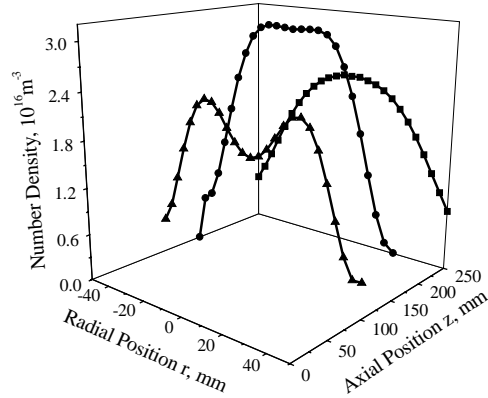


Fig. 4 Number density distribution of OI ( $3s^5S_2$ ) in the JUTEM arc-heater plume

At  $z=100$ mm, the peak of number density is located off axis at  $r=24$ mm. Then, the peak approaches to the axis in the downstream of the plume and finally the peak is located on the axis at  $z=250$ mm. The maximum number density in each plane increases up to  $3 \times 10^{16} m^{-3}$  at  $z=150$ mm and then decreases.

The number density distribution of metastable atomic oxygen in the university of Tokyo arc-heater plume is shown in Fig. 5. Similarly to the JUTEM arc-heater plume, the peak is also located off axis at the exit of the nozzle, and then the peak approaches to the axis in the downstream of the plume with the increase in number density.

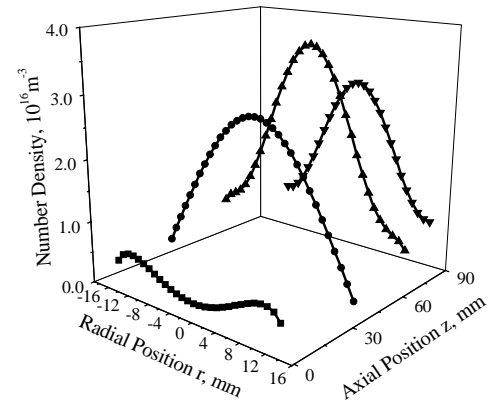
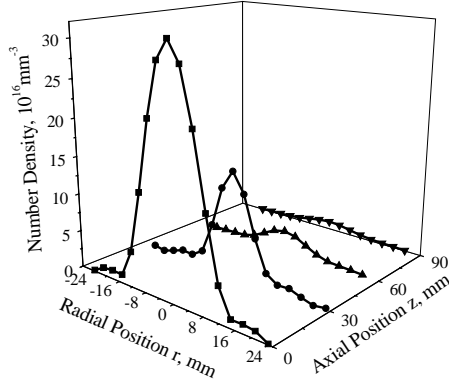


Fig. 5 Number density distributions of OI ( $3s^5S_2$ ) in

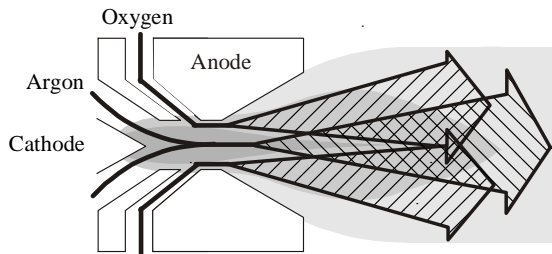
### the University of Tokyo arc-heater plume

Figure 6 shows the number density distribution of metastable argon. (It was measured using an ArI ( $4s^2[1/2]$ ) absorption line at 842.82nm.) It has a peak on the axis at the nozzle exit and then the number density decreases rapidly in the downstream of the plume.



**Fig. 6** Number density distribution of ArI ( $4s^2[1/2]$ ) in the University of Tokyo arc-heater plume

Consequently, oxygen is localized off axis near the nozzle exit and diffuses to the axis in the downstream region while it is dissociating. On the other hand, the metastable argon number density has a peak on the axis at the nozzle exit and decreases rapidly due to quenching in the downstream region. Therefore, it is thought that oxygen is not enough mixed with argon and not dissociated in the constrictor region. The hypothetical oxygen-argon mixing process in the plume is schematically shown in Fig. 7.



**Fig. 7** Hypothetical oxygen-argon mixing process

### 2.3 CFD Model

The number density of ground state atomic oxygen is difficult to be deduced from that of metastable state one because its electronic excitation would not be in equilibrium. Therefore, it was estimated by CFD simulations. In the conventional CFD analyses on an arcjet type arc-heater,<sup>13,14)</sup> oxygen mixing process has not been taken into account.

#### 2.3.1 Numerical models

Since the simulation focuses on the diffusion and mixing processes of the oxygen injected at the constrictor part, arc discharge process has not been solved for simplicity. The temperature distribution of the inlet argon flow was given as a boundary condition

assuming thermo-chemical equilibrium. This assumption would be valid because the flow speed is subsonic and pressure is high in the region around the cathode tip. The temperature profile has a sharp peak on the axis to simulate the cathode jet phenomena.

Seven species and seven chemical reactions model is used in this calculation as listed in Table 2. Arrhenius type forward reaction rates were used and the principle of the detailed balance was used to have backward reaction rates. One temperature model is employed.

**Table 2** Chemical reaction models.

Reaction process	Reference
$\text{Ar} + e \rightleftharpoons \text{Ar}^+ + e + e$	(15)
$\text{O}_2 + \text{Ar} \rightleftharpoons \text{O} + \text{O} + \text{Ar}$	(15)
$\text{O}_2 + \text{O} \rightleftharpoons \text{O} + \text{O} + \text{O}$	(16)
$\text{O}_2 + \text{O}_2 \rightleftharpoons \text{O} + \text{O} + \text{O}_2$	(16)
$\text{O} + e \rightleftharpoons \text{O}^+ + e + e$	(16)
$\text{O} + \text{O} \rightleftharpoons \text{O}_2^+ + e$	(16)
$\text{O} + \text{O}_2^+ \rightleftharpoons \text{O}_2 + \text{O}^+$	(16)

Viscosity, thermal conductivity and diffusion coefficient were calculated by the formulas in reference 16. In the free jet region, the algebraic turbulence model by the Plandtl's mixing length theory was used. The Reynolds number at the nozzle exit was 1800.

#### 2.3.2 Governing Equations

The fundamental equations are two-dimensional axisymmetric Navier-Stokes equations extended to chemical nonequilibrium gases.

The convection terms were calculated using the SHUS in which the spatial accuracy is extended to third order using the MUSCL approach. Implicit time integration has been done using the LU-SGS.

#### 2.3.3 Computation conditions

The schematic of computational grid for the University of Tokyo arc-heater plume analysis is shown in Fig. 8. A similar grid was used for the JUTEM arc-heater plume analysis. The calculation region is composed of two sections; the constrictor-nozzle section and the free jet section. At the interface of these sections, several computational grids were superposed to preserve the spatial accuracy. Since entire region in the constrictor and nozzle is covered by boundary layers, it is not necessary to concentrate the grid points near the wall surface.

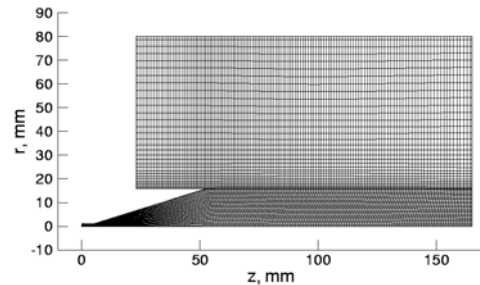


**Fig. 8 A computational grid**

The operational conditions listed in Table 1 are used for the computations. The inlet velocity of argon flow is subsonic so that the inlet pressure is extrapolated from the inside of constrictor. The pressure extrapolation is also done at the oxygen injection slit. To simulate the high temperature cathode jet, the Gaussian temperature distribution is assumed at the inlet as shown in Fig.9. The degree of ionization of argon at the inlet was computed assuming the Saha equilibrium. As for the wall of the constrictor, nozzle and chamber, adiabatic non-slip wall conditions were used.

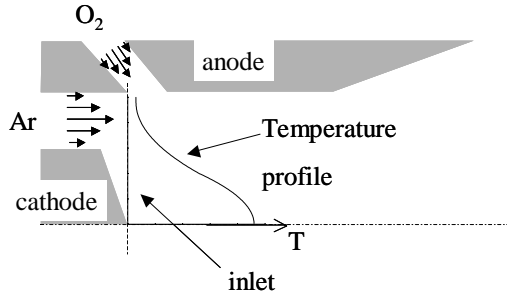


**Fig. 9 Gas inlet conditions**

## 2.4 CFD results

The radial distributions of  $O_2$  mole fraction, temperature and  $O$  mole fraction at 10 mm downstream from the cathode tip in the JUTEM arc-heater are plotted in Fig. 10.

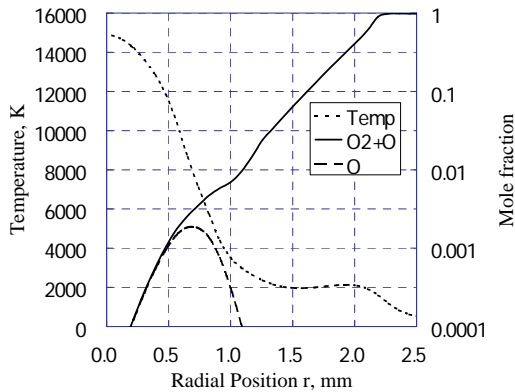


**Fig. 10 Radial distributions of temperature and oxygen mole fractions in the constrictor**

Since oxygen mixing is very slow, oxygen concentration is localized outside part of the plume in the constrictor. On the other hand, the temperature distribution still has a peak on the axis. Although the degree of dissociation is high in the region of  $r < 0.7$  mm, number density of atomic oxygen is very small. The average degree of dissociation at this cross section is as small as 0.01%.

The computed number density distribution of atomic oxygen in the JUTEM arc-heater plume is shown in Fig. 11. It corresponds to the case as previously shown in Fig. 4. The distribution has a peak at  $r=20$  mm and the peak approaches to the axis in the downstream of the plume.

The maximum number density in each plane increases from  $z=100$  mm to 150 mm. Consequently, localized oxygen distribution was also obtained in the simulation. This would be the reason why the measured metastable oxygen distribution has a peak off axis.

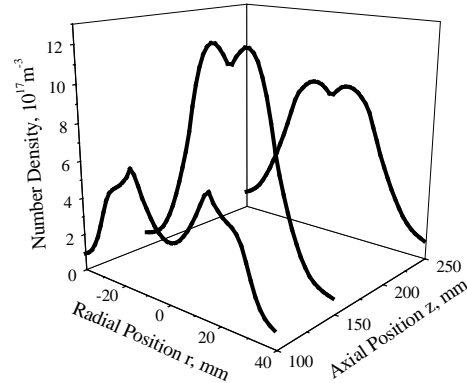


**Fig. 11 Computed number density distribution of atomic oxygen in the JUTEM arc-heater plume.**

The similar results were obtained for the university of Tokyo arc-heater plume. Figure 12 shows the computed contours of number density of atomic oxygen in the university of Tokyo arc-heater plume. Although the oxygen is mixing in the plume, the reaction rate is quite small because of the decrease in temperature. The atomic oxygen number density did not increase very much. The average dissociation degree of the oxygen in the plume was estimated at 0.01%.

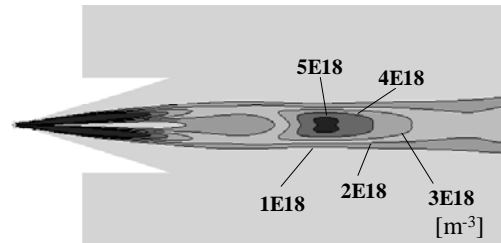


**Fig. 12 Computed contours of number density of atomic oxygen in the university of Tokyo arc-heater plume**

## 3. New Arc-heater

As mentioned above, the experimental and numerical results show that in the conventional arcjet type arc-heater plumes, oxygen is not enough mixed with argon and not dissociated in the constrictor region resulting in the low number density of atomic oxygen. Therefore, for the enhancement of the oxygen dissociation, the oxygen injection-port was improved so as that oxygen passes through a cathode-jet high temperature region in two new arc-heaters. In both arc-heaters, the oxygen mass flow rate is variable and the other operational conditions are same as those in Table 1.

### 3.1 New Arc-heater I

Firstly, the oxygen injection-port was shifted to the

upstream as much as possible. As shown in Fig.13, the length of the insulator made of boron (slash region) was variable, so that the oxygen injection-port can be optimized.

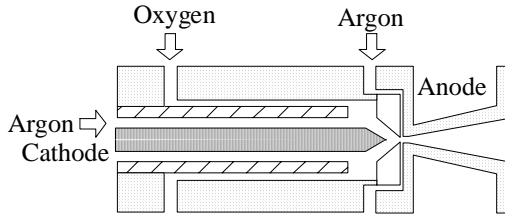


**Fig. 13 Oxygen injection part in new arc-heater I**

The absorption profile was strongest when the oxygen injection-port was 5mm from the cathode tip. Typical absorption profiles in new arc-heater I and conventional arcjet type arc-heater are shown in Fig.14. In this case, the number density of meta-stable oxygen was four times as high as that in the conventional arc-heater plumes, despite the low mass flow rate of 0.1slm. Since the translational temperatures in both arc-heaters are very close as shown in Fig.14 and the population temperatures in both arc-heaters would then be close, the degree of dissociation of oxygen in the new arc-heater 1 might be more than one order higher than that in the conventional one. However, in the arc-heater, the arc-discharge and the plume emission are very unstable and the operation can be conducted only a few minutes.

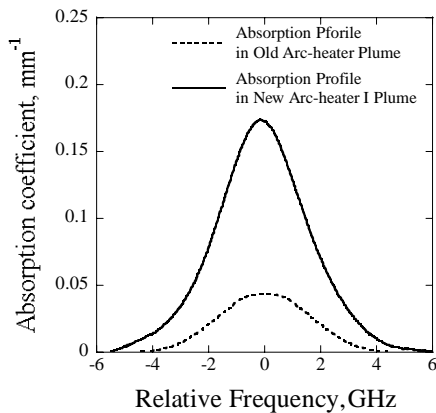


**Fig. 14 Absorption profile in new arc-heater I and conventional arcjet type arc-heater plumes**

### 3.2 New Arc-heater II

To make plumes stable, the oxygen was supplied through the hollow cathode tip as shown in Fig.15. At the oxygen mass flow rate of 0.2 slm, the plume was kept stable. Number density distribution of meta-stable oxygen and translational temperature distribution at the nozzle exit along with those in the conventional arcjet type arc-heater are shown in Figs.16, 17.

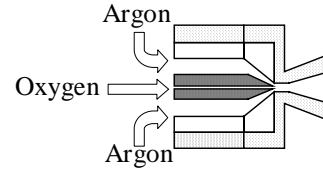


**Fig.15 Oxygen injection part in new arc-heater II**

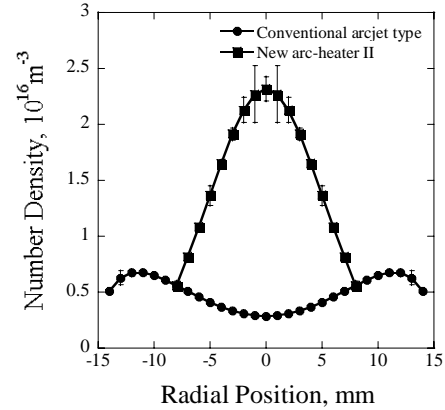


**Fig.16 Number density distributions in new arc-heater II and conventional arcjet type arc-heater plumes**

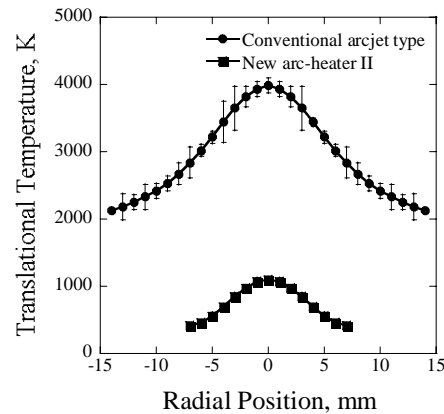


**Fig.17 Translational temperature distributions in new arc-heater II and conventional arcjet type arc-heater plumes**

The number density distribution in the new arc-heater II plume has a peak on the centerline. The maximum number density is four times as high as that in the conventional arcjet type arc-heater plume, which corresponds to be one order higher considering the mass flow rate of oxygen. On the other hand, the translational temperature in the new arc-heater II plumes is around 1100K, which is much lower than that in the conventional one.

This would be due to that the input enthalpy to the new arc-heater II is used for dissociation of oxygen much more than that to the conventional one. The low translational temperature also indicates the low electronic excitation temperature. Therefore there is a possibility that the number density of the ground state oxygen in the new arc-heater II plume is much higher than that in the conventional one, though that of meta-stable in the new arc-heater II is the same order as

that in the conventional one.

### CONCLUSION

- The distributions of metastable and total atomic oxygen number density were obtained by the laser absorption spectroscopy and the CFD simulation, respectively.
- Oxygen injected at the constrictor is found not enough mixed with argon in the constrictor, resulting in the quite small degree of dissociation of oxygen in the plume.
- Two new arcjet type arc-heaters, whose oxygen injection-ports were improved, were developed.
- As a result, in the new arc-heater II plumes, the plumes were kept stable. Since the translational temperature is low and then, the electronic excitation temperature is also thought to be low, the degree of dissociation of oxygen would become higher

### REFERENCE

- 1) Nishida, M. and Watanabe, Y.: Preliminary Experiments of Atomic Oxygen Generation for Space Environmental Testing, *Trans. Japan Soc. Aero. and Space Sci.*, Vol.31, No.93 (1998), p123-133.
- 2) Ishii, M., Ito, M., Toki, K. and Kuriki, K.: Atomic Oxygen Flow Facility Using Arcjet, Proceedings of 16 th Int'l Symp. on Space Tech. and Sic., Vol.1 (1988), p363-368.
- 3) Auweter-Kurtz, M., Kurtz, H. and Laure, S.: Plasma Generators for Re-Entry Simulation, *Journal of Propulsion and Power*, Vol. 12, No. 6 (1996), pp.1053-1061.
- 4) Salinas, I. T., Park, C., Strawa, A. W., Gopaul, N. and Taunk, J. S.: Spectral Measurements in the Arc Column of an Arc-Jet Wind Tunnel, AIAA Paper 94-2595, 1994.
- 5) Hinada, M., Inatani, Y., Yamada, T. and Hiraki, K.: An Arc-Heated High Enthalpy Test Facility for Thermal Protection Studies, ISAS-RN-664.
- 6) Hirakawa, M., Abe, K., Nishida, M., Takeishi, K. and Itoh, K.: Measurement of emission spectra from a shock layer of a blunt body in arc-heated gas, AIAA Paper 2001-1760, 2001.
- 7) Lago, V., Lebehot, A., Dudeck, M., Pellerin, S., Renault, T., and Echegut, P.: Entry Conditions in Planetary Atmospheres: Emission Spectroscopy of Molecular Plasma Arcjets, *Journal of Thermophysics and Heat Transfer*, Vol. 15, No. 2 (2001), pp.168-175.
- 8) Winter, M. W. and Auweter-Kurtz, M.: Boundary Layer Investigation in front of a Blunt Body in a Subsonic Air Plasma Flow by Emission Spectroscopic Means, AIAA paper 98-2460, 1998.
- 9) Storm, P. V. and Cappelli, M. A.: Laser-induced fluorescence measurements within an arcjet thruster nozzle, AIAA Paper 95-2381, 1995.
- 10) Kurotaki, T.: Construction of Catalytic Model on SiO<sub>2</sub> Based Surface and Application to Real Trajectory, AIAA Paper 2000-2366, 2000.
- 11) Arroyo, M. P., Langlogis, S. and Hanson, R. K.: Diode-laser absorption technique for simultaneous measurement of multiple gasdynamic parameters in high-speed flows containing water vapor, *Applied Optics*, Vol. 33 (1994), pp.3296-3370.
- 12) Zhang, F. Y., Komurasaki, K., Iida, T., and Fujiwara, T.: Diagnostics of an argon arcjet plume with a diode laser, *Applied Optics*, Vol. 38 (1999), pp1814-1822
- 13) Auweter-Kurtz, M., Goltz, T., Habiger, H., Hammer, F., Kurtz, H., Riehle, M. and Sleziona, C.: High-Power Hydrogen Arcjet Thrusters, *Journal of Propulsion and Power*, Sep., Vol.14, No.5 (1988) , pp. 764-773.
- 14) Matsuzaki, R. and Hirabayashi, N.: Some Characteristics of the Arc-Heater, Nozzle Flow, and the Underexpansion Jet in the NAL 60kW Plasma Wind Tunnel, NAL TR-307.
- 15) Matsuzaki, R.: Quasi- One-Dimensional Aerodynamics with Chemical, Vibrational and Thermal Nonequilibrium, *Transactions of Japan Society of Aeronautics and Space Science*, Vol.30, No.90 (1988), pp243-258.
- 16) Guputa, R. N. Yos, J. M. Thompson, R. A., and Lee, K. P.: A Review of Reaction Rates and Thermodynamic and Transport Properties for an 11-Species Air Model for Chemical and Thermal Nonequilibrium Calculations to 30000K, NASA R.P 1232, 1990.